be the particle energy due to field mixing

$$(r_1/r_0)^2(B_z^2/8\pi n)\cong 0.5 \text{ kev},$$

one finds $(r_1/r_0)^2$ and $\Omega\cong 2-5\times\Omega_0$ which is of the right order of magnitude.

The comparison between the experimental data on the fission instability and the above calculations support the hypothesis that the dissipation of the reversed trapped field is responsible for both the instability and the observed electron temperatures. Consideration of Eqs. (4) and (12) show that one can expect this instability to appear in situations where $r_1/r_0\sim 1$ if there is some mechanism which causes the reverse field to transfer its energy to the plasma. The time scale for such dissipation will increase with increasing plasma radius if the resistivity is given by the conventional Spitzer formula. However, if the fields interdiffuse rapidly due to some other instability of the reverse current sheet, the fission mode may appear early in time even in experiments where the plasma radius is relatively large.

However, experimental observations[1] of the time at which the fission mode appears in coils of various lengths show that the stable time can be increased by increasing the coil length. With longer coils the confinement time is increased because end losses are decreased[10] and this results in a larger plasma radius at a given time. These observations suggest that the time over which the field mixing occurs increases with r_0 and that perhaps the onset time of the fission instability can be delayed by appropriate scaling.[14]

ACKNOWLEDGMENT

We would like to express our appreciation to Dr. Marshall Rosenbluth for his essential criticism and suggestions.

[14] *Note added in proof.* This instability has not yet been observed in PHAROS, a larger experiment (coil length 180 cm, diameter 10.5 cm, $H_{\max}=80$ kgauss in 9 μsec, plasma radius 1.7 cm at peak field) with an initial reverse field of -3.8 kgauss. [A. C. Kolb, H. R. Griem, W. H. Lupton, D. T. Phillips, S. A. Ramsden, E. A. McLean, W. R. Faust, and M. Swartz, *Conference on Plasma Physics and Controlled Nuclear Fusion Research, Salzburg, Austria, September, 1961*, Nuclear Fusion J. (to be published)].

PHYSICAL REVIEW VOLUME 124, NUMBER 4 NOVEMBER 15, 1961

High-Voltage Glow Discharges in D_2 Gas. I. Diagnostic Measurements*

G. W. McCLURE
Sandia Corporation, Albuquerque, New Mexico
(Received July 10, 1961)

Pulsed glow discharges in D_2 gas at currents of the order of 1 amp and voltages in the range 40–80 kv are experimentally examined to determine the mass and energy distribution of ions incident on the cathode, the secondary electron emission due to various particles incident on the cathode, the energy spectrum of the electrons incident on the anode, the potential distribution along the glass walls, and the temperature and density of the electrons in the plasma which develops in the anode end of the discharge. The experimental results are discussed together with available cross-section data from the literature to establish the relative importance of the various collision processes which contribute to the sustainment of the discharge. Several processes peculiar to the extremely high operating potential (not of particular importance in ordinary glow discharges) are shown to assume dominant roles. These include electron backscattering from the anode, ionization of the gas by fast ions and fast neutral atoms, and ionization in the plasma region due to the secondary electrons released from the glass walls. The necessity of a complete revision of the usual theoretical point of view regarding electron ionization in the cathode region of the discharge and in the anode (plasma) region is indicated.

I. INTRODUCTION

IT has been shown by Pokrovskaia[1] that extremely intense glow discharges, conducting currents of 100 amp at applied potentials of 15 kv, exist under quasi-steady (pulsed) conditions in hydrogen gas. These discharges were observed between plane parallel electrodes 1.6 cm apart at a gas pressure of 0.21 mm Hg. Using five times larger electrode spacings and fivefold lower pressures, Pollock[2] found that 1- to 10-amp glow discharges could be sustained in deuterium for several μsec at potentials of the order of 100 kv. This discovery led to the development of compact neutron source tubes, filled with deuterium (D) or tritium (T) gas and fitted with D- or T-loaded cathodes, which produce neutron yields of $\sim 10^5$ per μsec for several tens of microseconds.[3]

The conditions of voltage, current, and pressure under which these discharges operate are apparently beyond the realm of applicability of existing glow discharge theories. Neu[4] has presented a theoretical discussion of high-current, high-voltage discharges which introduces many applicable concepts, but there is reason to believe

* Work performed under the auspices of the Atomic Energy Commission.

[1] A. S. Pokrovskaia and B. N. Kliarfel'd, Soviet Phys.—JETP **5**, 812 (1957).

[2] H. C. Pollock, General Electric Research Laboratories, Schenectady, New York (private communication, April, 1957).

[3] R. D. Kelley, J. C. Hamilton, and L. C. Beavis, Rev. Sci. Instr. **32**, 178 (1961).

[4] H. Neu, Z. Physik **155**, 77 (1959).

that the theory requires modification for treating the Pollock discharge.

In this theory Neu invokes the experimental fact that high-current discharges at potentials up to a few kilovolts are separated into a plasma region adjacent to the anode and a "cathode-fall" or positive ion sheath between the plasma and the cathode. It is assumed that secondary electrons released from the cathode by positive ion and fast neutral atom impact multiply exponentially with distance as they cross the cathode fall, and that ionization in the cathode fall due to fast ions and fast neutral atoms is negligible compared with that due to electron impact.

From the observed neutron yields of the Pollock tubes, it can be estimated that the mean energy of the ions and atoms incident on the cathode is of the order of 10–20 kev. Under such conditions ionization of the gas due to ions and fast neutrals is surely an important effect. The *field strength to pressure* ratio required to impact such high energies to the ions, considering the retarding effect of charge exchange, is $\sim 10^5$ v/cm-mm Hg. In such high fields, electrons from the cathode probably do not produce simple exponentially increasing avalanches since the electron velocity can become very large.

It has been previously suggested that fast electrons backscattered from the anode appreciably augment the ionization in high-voltage discharges.[5,6] Such an effect has never been taken into account in a unified quantitative theory. The backscattering of electrons to the insulating walls in a Pollock-type discharge almost certainly has an important influence on the initial buildup of the discharge the steady-state potential distribution along the walls, and the configuration of the plasma if a plasma actually exists.

To obtain more direct evidence of the pertinence of the above discussed processes to the Pollock-type discharge, a number of diagnostic experiments have been performed on pulsed glow discharges in D_2 gas at potentials of 40–80 kv and currents of 0.5 to 7.0 amp. It is the main purpose of this paper to describe the methods and results of these experiments.

The study includes determinations of (1) the voltage-current characteristics of the discharges at various pressures, (2) the effect of anode material on the voltage-current characteristics, (3) the mass, energy, and angular distribution of the ions incident on the center of the cathode, (4) the secondary emission coefficient vs energy for the principal ions incident on the cathode, (5) the relative contribution of ions and neutrals to the total secondary electron production at the cathode, (6) the energy and angular distribution of the electrons incident on the anode, (7) the distribution of potential along the glass walls of the active discharge, (8) the temperature and density of slow electrons in the plasma which is found to develop near the anode, and (9) the physical length of the plasma.

The experimental data, interpreted with the aid of cross-section data from the literature, provide considerable insight regarding the modes of ion generation and electron and ion motion in various parts of the discharge. In a later paper (Part II), use is made of the conclusions of the present investigation to construct a detailed one-dimensional theory of the cathode fall region of the discharge.

Throughout the discussion, extensive use is made of cross-section data for hydrogen ions and fast neutrals. This has been forced by unavailability of deuterium data on many of the pertinent types of collision process. In all cases where substitutions are necessary it is assumed that a deuterium ion or neutral of a given energy behaves exactly as the corresponding hydrogen species of half this energy. The validity of this assumption has been proven in practically every instance where direct comparisons of the two isotopic species have been made.[7–10]

In calculations of the ionization of D_2 by electrons, we use the cross section vs energy relation for electrons on H_2. Although there is evidence that the cross sections for dissociative ionization of H_2 and D_2 by electron impact are unequal,[11] this process appears to have a negligible probability as compared with simple electron removal to form the molecular ion. The dissociative ionization process is therefore ignored.

It is tacitly assumed that the concentration of dissociated deuterium which develops during the discharge process is negligible compared to that of D_2 gas molecules. The total number of ions arriving at the cathode during one pulsed operation—a number roughly equal to the number of ions produced per discharge—is generally less than 10^{14}. By comparison, the number of gas molecules present is of the order of 10^{18}. Assuming that ionizing and dissociative collisions occur at roughly the same rates, it follows that the buildup of atomic D is negligible.

II. DISCHARGE TUBE AND POWER SUPPLY

The tube geometry used in all parts of the investigation consisted of a pair of flat metal electrodes spaced 7.6 cm apart within a 5.1 cm i.d. Pyrex tube. A 1.5-mm annular gap between the electrode edges and the glass walls allowed gas to flow freely from the inlet and outlet tubulations at the end of the Pyrex tube without permitting long-path breakdown into the space behind the electrodes. Minor design adaptations of the basic geometry for special diagnostic experiments are shown

[5] A. Dikidzhi and B. N. Kliarfel'd, Zhur. Tekh. Fiz. **25**, 1038 (1955).
[6] G. W. McClure, J. Electronics and Control **7**, 439 (1959).
[7] F. P. Ziemba, G. J. Lockwood, G. H. Morgan, and E. Everhart, Phys. Rev. **118**, 1552 (1960).
[8] S. F. Philp, J. Appl. Phys. **31**, 1592 (1960).
[9] A. Schmid, Z. Physik **161**, 550 (1961).
[10] W. L. Fite, R. T. Brackmann, and W. R. Snow, Phys. Rev. **112**, 1161 (1958).
[11] O. A. Schaeffer and J. M. Hastings, J. Chem. Phys. **18**, 1048 (1950).

in Figs. 4 and 12. In all of the experiments other than those of Sec. III, both electrodes were of polished 303 stainless steel.

The vacuum pumps permitted preliminary evacuation of the tubes to a pressure of 10^{-6} mm Hg. Deuterium gas supplied by the Stewart Oxygen Company, rated 99.5% pure, was used for backfilling. During tube operation, the gas was admitted continually through a slow leak and pumped out through a throttled opening to the vacuum pump. The resulting steady renewal of gas prevented an accumulation of the impurity gases released from the walls by ion and electron bombardment. The pressure was measured by means of a thermocouple gauge calibrated for D_2 gas against a precision McLeod gauge.

High-voltage pulses were supplied from a bank of four 0.1-μf capacitors. These were charged in parallel to one-fourth the desired pulse potential and discharged through a set of spark gaps to provide a quadrupling of the voltage. An automatic control circuit alternately charged the capacitors and discharged the stored energy through the experimental tube at the rate of four times per minute. The voltage and current pulses were viewed, respectively, by means of a 1000:1 capacitive voltage divider connected to the high-voltage tube terminal and a 1-ohm resistor connected in series with the grounded terminal. For the positive ion mass-energy analysis the cathode was operated at ground potential; in all other cases the anode was grounded. Typical voltage and current oscillograms are shown in Fig. 1.

The tubes were constructed with Teflon or rubber O-rings to facilitate replacement and adjustment of electrodes and to permit insertion of movable probes. As such construction would not permit bakeout at high temperature, the walls and electrodes were processed mainly by repeated discharging of the assembled tube. Initial outgassing was evidenced by abnormally high currents and occasional arc breakdown during the first few discharges; however, after several preliminary discharges, no further variations were observed in a sequence of several hundred successive discharges.

While failure to achieve complete outgassing gives rise to some residual gas contamination, the behavior of the discharge was not appreciably affected by the actual gaseous impurity levels encountered. A mass spectrometer analysis (obtained with the instrument described below) of ions emerging from a small cathode aperture showed the principal spurious ions at the start of a discharging sequence to be H^+, H_2O^+, CO^+, O^+, and N^+. When the total fraction of these ions relative to the principal ions D^+ and D_2^+ was reduced from 10% to below 1% by repeated discharging, no significant change occurred either in the total tube current or in the energy spectra of the principal ions.

Residual surface contamination made it impossible to precisely reproduce behavior in two similarly constructed tubes; however, admission of air and reprocessing of the same tube without touching the interior of the glass walls gave quite reproducible results.

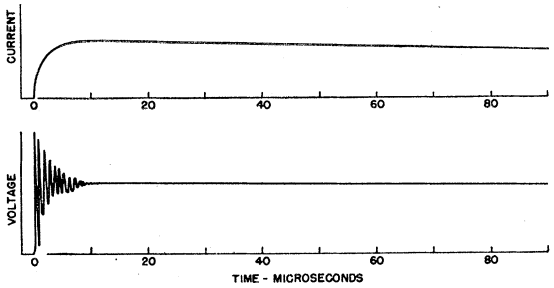

FIG. 1. Oscillograms of the total tube current and applied voltage vs time under the operating conditions used for the ion spectrum determinations. Peak current 0.8 amp, voltage after decay of the initial oscillation 80 kv, pressure 0.059 mm Hg. The damped oscillation appearing at the start of the voltage pulse is caused by stray inductance in the capacitor bank. An *R-C* low-pass filter ($R=1000$ ohm, $C=0.0025$ μf) was inserted between the capacitor bank and the tube to attenuate this initial oscillation. The buildup time of the discharge (inherently <1 μsec) is artifically increased by the shunt capacitance of the filter. All measurements reported in this paper are limited to the time interval during which the current is within 20% of peak value. The duration of this period varied from 200 μsec to 20 μsec depending on the magnitude of the peak current.

It is believed that the glass, rather than the electrodes, is responsible for variations in the tube behavior since in previous experiments where minimum glass area was exposed to ion bombardment[6] much better reproducibility was obtained. Unfortunately the more favorable geometry used in these earlier experiments could not be used at the present higher voltages because arc breakdown occurred very frequently when the minimum electrode spacing was reduced below ~ 5 cm.

III. VOLTAGE-CURRENT CHARACTERISTICS

A typical set of voltage-current characteristics for the discharge is shown in Fig. 2. The data were obtained for a tube having a titanium-coated stainless steel cathode loaded with deuterium gas. Relative neutron yields were measured by means of a liquid scintillation proton recoil detector which was lead shielded to eliminate response to x-rays. This detector gave a time-resolved reading of the instantaneous neutron production rate during the quasi-steady portion of each discharge. In the region investigated the curves of voltage (V_T) vs (I_T) are closely approximated by a simple "power-law" expression of the form

$$I_T = af(p)V_T^k, \tag{1}$$

where a and k are constants and $f(p)$ is a function of the pressure. From the cross plot, Fig. 3, of I_T vs p at constant voltage it is evident that $f(p)$ may also be roughly approximated by a power law of the form

$$f(p) = bp^m, \tag{2}$$

where b and m are constants. Over the range of these measurements $k=2.9\pm0.1$ and $m=2.6\pm0.2$.

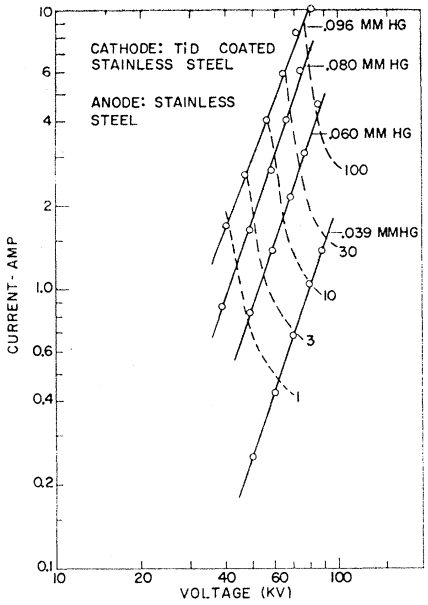

FIG. 2. Voltage-current characteristics of the discharge tube with a cathode coating of titanium deuteride. The dashed curves are lines of constant neutron yield labeled with numerals proportional to yield.

Pokrovskaia *et al.* have observed a V_T vs I_T dependence similar to Eq. (1) for H_2 discharges at 1–15 kv and 1–100 amp.[1] According to our analysis of their published data, the k value for their discharge is also 2.9.

Although a and b were observed to vary by as much as a factor of 2 for tubes of the same geometry and construction, k and m changed only slightly. The uncontrolled variations in a and b are believed to be due to changes in the secondary emission coefficient of the glass walls due to variations in occluded surface contaminants. In comparing the curves of Fig. 2 with operating conditions observed in other parts of the paper, it should be noted that the coated cathode used here probably had a different secondary emission coefficient than the plain stainless steel used in the remaining experiments.

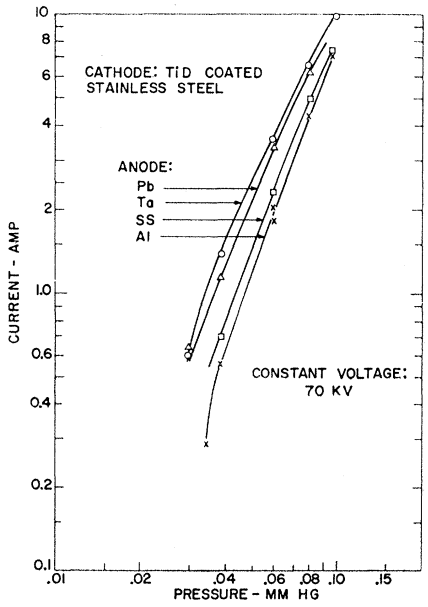

FIG. 3. Tube current vs pressure at constant voltage showing the effect of anode material on the gross characteristics of the discharge. *SS* represents stainless steel.

Figure 3 shows the result of varying the anode material. A very pronounced and reproducible effect is observed which is believed to be due to the variation of the electron backscattering coefficient of high-energy electrons as a function of the anode atomic number. This effect has been observed previously in measurements of the starting potential of discharges below the Paschen minimum.[5,6] The backscattering of electrons from the anode to the walls will be discussed at greater length in connection with the mechanism of ion generation in the plasma region of the discharge.

IV. ION ANALYSIS

The energy and mass distributions of ions incident on the cathode during the steady-state portion of the high voltage pulse were studied by means of the mass spectrometer shown in Fig. 4.

The data required for mass and energy spectrum determinations were obtained by varying the magnetic field in small steps from one discharge to the next. The electrostatic deflection voltage was varied linearly from zero to 3 kv so as to scan the entire ion energy spectrum during a 50-μsec steady portion of each discharge. The current signal received by the collector behind *S*4 was amplified by a wide-band amplifier (0.1-μsec rise time)

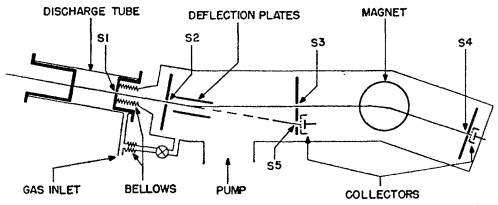

FIG. 4. Schematic diagram of mass spectrometer with discharge tube attached. The instrument consists of an electrostatic analyzer for selecting ions in a narrow energy band and a magnetic analyzer for splitting the resultant monoenergetic beam into separate mass components. Ions from the discharge enter the spectrometer through a 0.020-in. hole *S*1 in the center of the cathode. A gimbal and metal bellows connecting the tube base with the body of the spectrometer permit the tube to be tilted in two degrees of freedom so that any portion of the ion beam within ± 3.5 degrees of the tube axis can be directed through the 0.010-in. slit *S*2 into the electrostatic analyzer. The gimbal is arranged with its center of rotation located at the center of aperture *S*1 so that variations of the tilt angle do not change the calibration of the energy analyzer. Energy selection occurs at a 0.040-in. wide rectangular slit *S*3 which receives ions electrostatically deflected through an angle of 4.7 degrees. Ions transmitted through *S*3 are momentum-resolved by a 0.25-in. wide rectangular slit *S*4 located to receive ions magnetically deflected through an angle of 18.4 degrees. The slit widths were chosen so that the resolution of the instrument was sufficient to separate adjacent atomic masses up to mass 10 amu.

and applied to the vertical plates of an oscilloscope while a voltage proportional to the spectrometer electrostatic deflection voltage was applied to the horizontal plates. This type of data display is especially convenient since a nearly linear relation exists between the horizontal deflection and the energy of the ions producing the vertical deflection.[12] Since the magnetic analyzer acts as a momentum selector, ions of unlike mass appear at different positions on the display trace. Several typical oscillograms are shown in Fig. 5.

The differential energy spectra were determined from the envelopes traced out by the tops of the individual mass peaks as the magnetic field was varied from one discharge to the next. The only corrections applied were (1) a correction for energy scale nonlinearity,[12] (2) multiplication of the spectra by a factor proportional to ion energy to compensate for the linear variation of the energy bandwidth with ion energy, and (3) a small correction for dependence of amplifier gain on pulse width. No correction for collector secondary electron emission was required as a positive bias sufficient to suppress all secondaries was applied to the collector.[13]

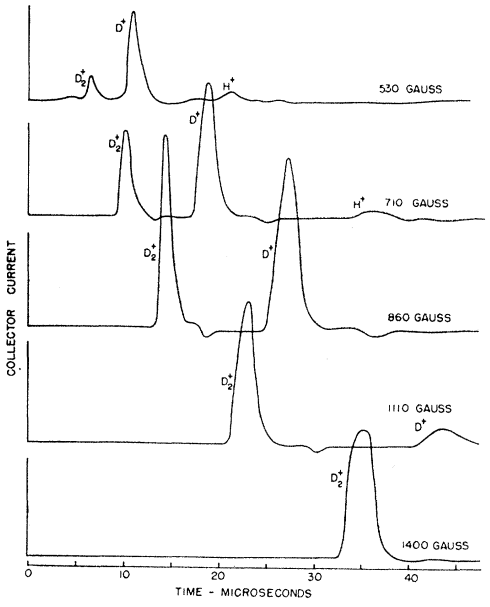

FIG. 5. Mass spectrum oscillograms recorded at several values of the magnetic analyzer field. Each of these records was obtained under the same tube operating conditions as Fig. 1. The horizontal position of the peaks is (except for a small deviation noted in the text) directly proportional to the ion energy. Knowledge of the energy of the ions in each peak together with the particle momentum, determined from the magnetic field setting, suffices to establish the mass species responsible for each peak. Small traces of H^+ impurity ions are seen in the top two traces.

[12] A slight nonlinearity is introduced by the mass- and energy-dependent transit time of ions from the electrostatic deflection plates to the collector. Corrections for this effect are simple and straightforward.

[13] Attraction of secondary electrons from the front surface of slit $S4$ to the collector was eliminated by placing a negatively biased grid between the collector and slit $S4$.

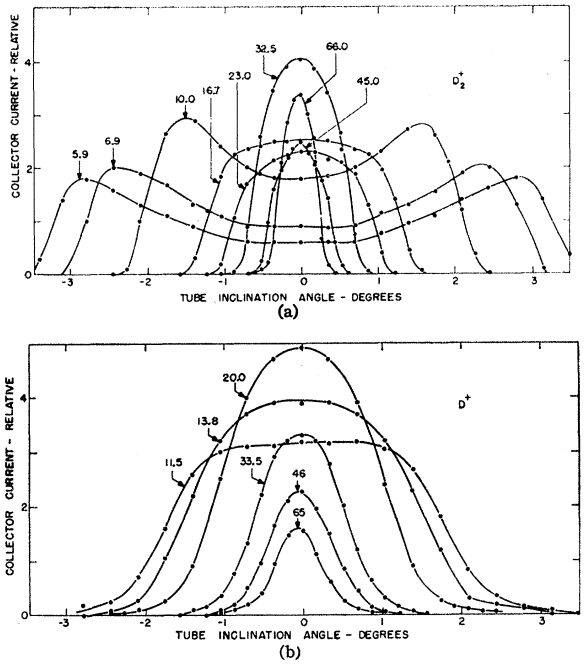

FIG. 6. Angular distributions of D_2^+ ions (a) and D^+ ions (b) emergent from 0.020-in. cathode aperture. Curve parameter refers to kinetic energy of ions in kev units. All curves apply to the same operating conditions as Fig. 1.

A 500-liter/sec oil diffusion pump provided a vacuum of 1.5×10^{-6} mm Hg in the spectrometer when the discharge tube was operated at 0.060 mm Hg. Subsidiary tests showed that the ion beam was not significantly attenuated or scattered within the spectrometer.

With the tube operating at a potential of 80 kv and a current of 0.8 amp (gas pressure 0.059 mm Hg), the results shown in Figs. 6 and 7 were obtained. Figure 6 gives the angular distributions of the D^+ and D_2^+ ions as a function of energy and Fig. 7 gives the differential energy spectra of the D^+ and D_2^+ ions integrated with respect to solid angle of emergence from $S1$. Below the lower energy limits of 5 kev for D_2^+ and 10 kev for D^+, the spectra could not be determined because the angular spread of the ions exceeded the available range of the tilt angle adjustment. Significant points regarding the results are as follows: (1) All spectra have a sharp intensity cutoff at the energy corresponding to free fall from anode to cathode (80 kev in this case). (2) Both the D^+ and D_2^+ ions have a mean energy of the order of 25% of this maximum energy. (3) The D^+ spectrum has a relative maximum at 15 kev while the D_2^+ spectrum decreases monotonically over the whole measured range. (4) Above 20 kev the shapes of the D^+ and D_2^+ spectra are quite similar. (5) The ratio of the total output of D^+ to that of D_2^+ is 0.54 in the spectral energy range 10 to 80 kev.

A small but definite trace ($\sim1\%$) of the ions is of the D_3^+ species. These ions, unlike the D^+ and D_2^+ species, have a discrete energy spectrum consisting of a sharp

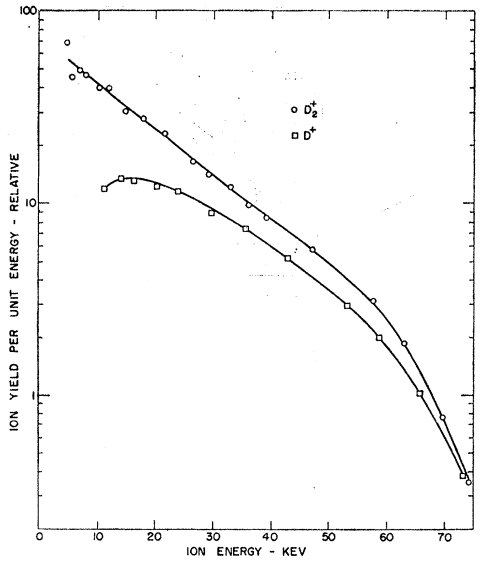

FIG. 7. Differential energy distributions of D_2^+ and D^+ ions emergent from 0.020-in. cathode aperture. Operating conditions same as in Fig. 1.

peak at 80 kev indicating that D_3^+ is formed only in portions of the tube where the space potential is near anode potential. The plasma region (Sec. IX) is the most likely source of D_3^+.

The angular divergence of the ion beam emergent from the cathode aperture (Fig. 6) is believed to arise primarily from the following three effects: (1) space charge mutual repulsion, (2) radial electric field components in the neighborhood of the ion exit aperture, and (3) repulsive molecular forces active during the dissociation of molecular ions within the discharge. In order to estimate the contribution of space charge, the total ion current incident on the front surface of $S2$ was measured (with secondary electron emission suppressed by a biased grid). This current was 1.67×10^{-4} amp under the 0.8-amp, 80-kv operating condition. Using ion velocity spectra deduced from the D^+ and D_2^+ energy spectra, it is found that, for the observed total current, the charge density in the ion beam is sufficient to give rise to about half the observed D_2^+ angular divergence. The aperture defocusing effect (2) is estimated to add an additional divergence of about the same magnitude as the space charge effect. Thus, (1) and (2) account for the major part of the D_2^+ ion divergence.

Both (1) and (2) should theoretically give rise to an angular divergence inversely proportional to ion energy and independent of mass. While this effect is observed in the case of the D_2^+ ions, the D^+ ions not only have, at each energy, a much broader divergence than D_2^+ ions of the same energy but the D^+ ions do not follow the inverse energy relationship. This effect can be accounted for by the fact that some if not all of the D^+ ions arise from excitation of D_2^+ ions to 1 $^3\Sigma_u$ states. When so excited, the D_2^+ ion dissociates and the D and D^+ components are driven apart by a repulsive force which imparts ~5 ev to each particle in the center-of-mass coordinate system. This results in an additional angular spread for D^+ ions over and above (1) and (2), which accounts quantitatively for the differences between the D^+ and D_2^+ maximum angles of divergence.

The total ion current through the aperture $S1$, mentioned above, corresponds to an ion current density of 0.083 amp/cm^2 at the center of the cathode. Assuming an average secondary electron emission per ion of 14.1 (see Sec. VI), the total current density, including secondary electrons, is 1.25 amp/cm^2. Since the total tube current was 0.8 amp, it may be concluded that the current density at the center of the cathode is 31 times the average current density over the cathode surface. If the total current were concentrated in a core of uniform current density, the diameter of this core would be 0.90 cm. This corresponds very closely to the diameter of a visible core of reddish color which is quite intense close to the cathode and fades off gradually into a general bluish background at a distance of ~2 cm from the cathode. Examination of this core via time-resolved spectroscopy indicated the presence of the spectral lines of atomic deuterium (4861 and 6563 A) superimposed on a continuous spectrum. The atomic lines were detectable above background only in this core and only out to ~2 cm from the cathode. The concentration of atomic deuterium in this region is believed to be due to the dissociation in flight of fast D_2^+ ions and fast D_2 neutrals. From the plasma and wall potential measurements it will be seen that the length of the reddish core corresponds approximately with the extent of the high-field or cathode-fall region wherein the ions gain sufficient energy to give rise to the above processes.

V. SECONDARY EMISSION COEFFICIENTS OF D^+ AND D_2^+

The secondary emission coefficients of D^+ and D_2^+ ions in the energy range 10–80 kev were determined in the course of the mass spectrum measurements by observing the heights of the mass peaks as a function of the collector bias. The peaks saturated in height at biases less than -30 v and greater than $+90$ v. The ratio of the maximum height at -30 v bias to the minimum height at $+90$ v bias was assumed to equal $\gamma+1$, where γ is the mean secondary electron yield per ion. In order that the results might be used to estimate the secondary yields of the ions impinging on the discharge tube cathode, the collector was made of the same material as the cathode (303 stainless steel). Results are shown in Fig. 8.

With some uncertainty as to the correspondence between the surface conditions of the collector and the discharge tube cathode, we have estimated the average cathode secondary yield per ion by averaging the γ

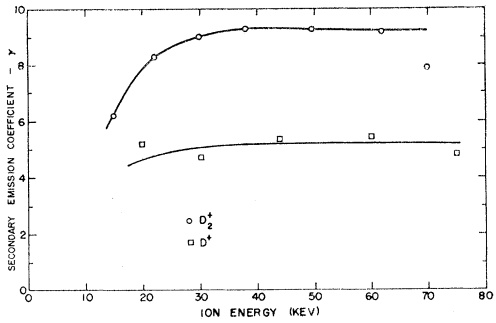

FIG. 8. Secondary emission coefficients, γ, of D_2^+ and D^+ ions incident on stainless steel as a function of ion kinetic energy.

values of Fig. 8 over the energy spectra of Fig. 7. Including both D_2^+ and D^+ ions of energy >10 kev, the average is $\bar{\gamma}=6.2$. The separate averages for the D_2^+ and D^+ species alone are 6.8 and 4.7, respectively. If one were to include the lower energy ions (<10 kev) these averages would be somewhat lower, since all available secondary emission data for light positive ions show a monotonically increasing dependence of γ on ion energy below 10 kev.[14–18]

VI. SECONDARY EMISSION DUE TO NEUTRAL PARTICLES

In collisions with gas molecules, the fast D^+ and D_2^+ ions may undergo the following transformations[9,19,20]:

$$D^+ + e \rightarrow D,$$
$$D_2^+ + e \rightarrow D_2,$$
$$D_2^+ + e \rightarrow 2D,$$
$$D_2^+ \rightarrow D + D^+,$$
$$D_2^+ \rightarrow 2D^+ + e.$$

The first three reactions involve the capture of an electron from a gas molecule and the last two involve simple dissociation. In all of these reactions the majority of the product particles proceed with essentially the same velocity and direction as the primary. The cross sections are of the order of 10^{-15} to 10^{-16} cm^2 in the energy range of interest in the present discharges and the corresponding mean free paths, for a pressure of 0.60 mm Hg, are roughly 0.6 cm to 6 cm. Hence, a large fraction of the D^+ and D_2^+ ions generated in the gas are converted to atomic or molecular neutrals before reaching the cathode. According to Schwirtzke,[20] atomic ions and the corresponding neutrals have comparable secondary emission coefficients; thus, a considerable fraction of the total secondary current in the present discharges must be due to neutrals.

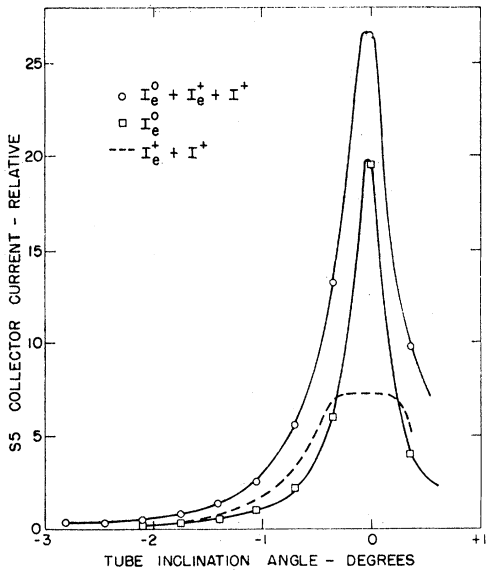

FIG. 9. Angular distribution of currents $I_e^0+I_e^++I^+$, I_e^0, and $I_e^++I_0^+$, indicating the relative contribution of positive ions and neutral particles to the release of secondary electrons at a collector ($S5$) directly aligned with collimating slits $S1$ and $S2$ of the mass spectrometer. Operating conditions same as in Fig. 1.

The mass spectrometer (Fig. 4) was used to determine indirectly the relative contribution of ions and neutrals to the total secondary electron current at the cathode. A slit $S5$ was placed in the plane of $S3$ and arranged to cover the solid angle subtended by the entrance slits $S1$ and $S2$. A stainless steel collector similar in construction to that located at $S4$ was placed immediately behind $S5$. With no deflection potential applied to the electrostatic analyzer plates, both the ions and neutrals emerging from $S2$ were received at the collector, but with a 1-kv deflection voltage only the neutrals were received. With the collector biased at a negative potential to eject secondary electrons, the following currents were measured: (1) I_e^0, the secondary electron current due to neutrals striking the collector, and (2) the composite current $I_e^0+I_e^++I^+$, where I_e^+ is the secondary electron current due to positive ions and I^+ is the positive-ion current. The results of the measurements, as a function of tube tilt angle, are shown in Fig. 9.

Integration of the angular distributions with respect to the emission solid angle shows that the total current of secondary electrons due to neutrals is 1.1 times the combined currents of positive ions and positive ion secondaries. Using the value $\bar{\gamma}=6.2$ for positive-ion secondary emission (Sec. V), it may be deduced that the effective secondary emission per positive ion, including emission due to neutrals, is 14.1. For future reference we designate this quantity as $\bar{\gamma}'$.

The extremely narrow angular distribution of the neutrals, indicated by the curve I_e^0 in Fig. 9, shows that

[14] V. G. Telkovskii, Soviet Phys. "Doklady" **1**, 334 (1957).
[15] S. N. Ghosh and W. F. Sheridan, J. Chem. Phys. **26**, 480 (1957).
[16] H. C. Bourne, R. W. Cloud, and J. G. Trump, J. Appl. Phys. **26**, 596 (1955).
[17] M. Helea and E. L. Chaffee, Phys. Rev. **49**, 925 (1936).
[18] M. Helea, Phys. Rev. **55**, 984 (1939).
[19] J. B. H. Stedeford and J. B. Hasted, Proc. Roy. Soc. (London) **A227**, 466 (1955).
[20] F. Schwirtzke, Z. Physik **157**, 510 (1960).

these particles move essentially in the direction of the electric field. This is consistent with the production mechanisms discussed.

VII. ELECTRON SPECTRUM AT THE ANODE

The energy distribution of the electrons incident on the anode of the discharge tube was measured using an electrostatic analyzer of the same dimensions as the left-hand section of the instrument shown in Fig. 4. Magnetic perturbations of the electron trajectories in the analyzer due to stray magnetic fields were eliminated by aligning the long axis of the analyzer parallel to the earth's magnetic field.

Using the same sweep deflection and oscillographic plotting technique as in the ion energy analysis, spectra of electrons emerging from a 0.020-in. central anode aperture were obtained over a range of tilt angles and integrated with respect to solid angle to give a complete energy spectrum. The final results are shown in Fig. 10 for a tube operating at 77 kv, 1.4 amp, 0.055 mm Hg. The sharp spike at the high-energy end of the spectrum represents the electrons which pass all the way from cathode to anode without suffering appreciable energy losses due to collision, and the low-energy continuum represents the electrons which are produced by ionizing collisions of electrons and fast ions along the length of the discharge. The small peak at 28 kev is a "ghost" of the monoenergetic 77-kev peak caused by diffraction at the edges of the electron collimating slit immediately in front of the deflection plates. Discounting the area of this spurious peak, the total number of electrons in the discrete peak at 77 kev is 6.6 times the number in the continuum below 70 kev.

This ratio is a rough indication of the number of secondary electrons released at the cathode per positive ion produced in the gas. There is a discrepancy, however, between this ratio so interpreted and the value of $\bar{\gamma}'$ from Sec. VI. Possible sources of the discrepancy are a focusing effect within the discharge which tends to

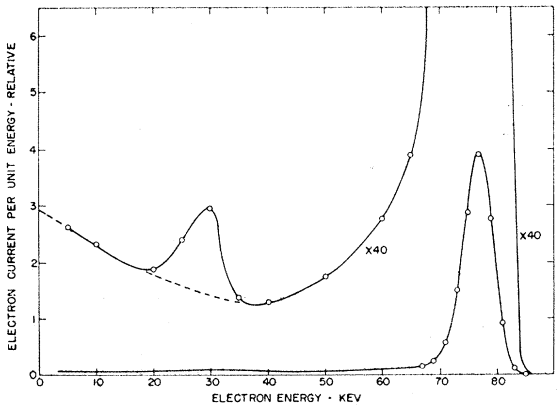

FIG. 10. Differential energy spectrum of electrons emergent from a 0.020-in. anode aperture. Tube voltage 77 kv, total tube current 1.4 amp, pressure 0.055 mm Hg.

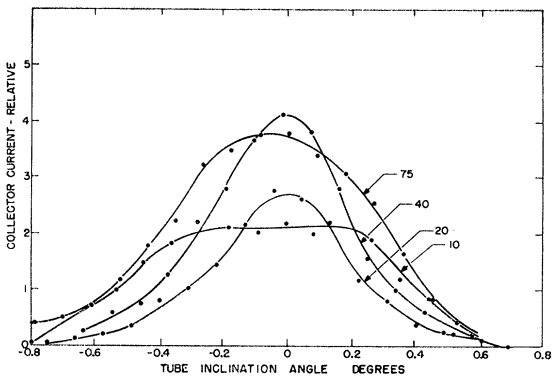

FIG. 11. Angular distributions of electrons emergent from 0.020-in. anode aperture. Curve parameter refers to electron energy in kev units. Operation conditions same as Fig. 10.

overemphasize the low-energy end of the measured electron spectrum, an overestimate of $\bar{\gamma}$ as calculated from the indirect secondary emission and the ion spectrum measurements, and/or an overestimate of the contribution of neutrals to the cathode secondary electron yield. No detailed analysis of these effects has been carried out; however, in the remaining part of the paper, it will be arbitrarily assumed that $\bar{\gamma}'=14.1$ as calculated in Sec. VI.

The angular distributions of the electrons emergent from the anode aperture are shown in Fig. 11. These distributions indicate that the electrons produced along the axial region, at points more than 10 kv negative relative to the anode, move nearly parallel to the tube axis suffering very little gas scattering.

VIII. WALL POTENTIAL DISTRIBUTION

The distribution of potential along the glass walls of the discharge tube was determined by means of the arrangement shown in Fig. 12. The potential sensing element was a ring-shaped stainless steel probe inserted so as to form a short (1.5 mm wide) section of the wall. The anode and cathode were mounted on rods which slid axially in O-ring seals so that both electrodes could be moved in relation to the ring probe. Using a fixed spacing of 7.6 cm between the anode and cathode, the floating potential of the probe during the steady-state portion of the discharge was determined as a function of distance from the anode. The potential measurements were made by means of a capacitive voltage divider consisting of a 15-$\mu\mu$f voltage dropping capacitor and a 0.015-μf voltage viewer capacitor.

Wall potential distributions for several pressures and voltages are shown in Fig. 13. Measurements could not be carried out on portions of the wall where the floating potential exceeded -20 kv relative to the anode, because in such locations the probe caused instabilities and frequent arc breakdown. At all other locations the wall potential was found to be negative with respect to the anode and the probe caused no disturbance. In

general a certain length of the wall in the anode end of the tube attains a potential within 1 kv of anode potential; however, at some point the potential begins to rise very rapidly with increasing distance from the anode. The effective location of this point for various operating conditions was determined by extrapolating the rising portions of the curves in Fig. 13 to the horizontal axis. By analogy with ordinary glow discharge terminology, we label the portion of the discharge between the starting point of the rise in wall potential and the cathode as the "cathode fall" region.[21] It is found that the length of the cathode fall d_c and the pressure p are related according to the following empirical expression:

$$pd_c = 0.216 \pm 0.010 \text{ mm Hg-cm.} \quad (3)$$

This relation is found to hold independently of tube voltage for potentials from 40 to 80 kv.

In "normal" and "abnormal" glow discharges a relation similar to Eq. (3) describes the extent of the cathode fall; however, the constant on the right is replaced by a voltage-dependent term. Presumably the voltage independence observed here is related to the extreme steepness of the starting potential vs pressure curve (Paschen curve) for very high voltages and low pressures.[1,6] The similarity between the conditions in the cathode fall region in a normal or abnormal glow discharge and the conditions at the onset of a self-sustained discharge, at operating conditions near the Paschen minimum, has been cited in nearly all gas discharge treatises. This similarity results from a positive space charge buildup terminating in the formation of a plasma or "positive column" in the anode end of the tube whenever the applied voltage exceeds the minimum value required for breakdown. In the steady state, the plasma of the low-voltage glow discharge is an inert buffer zone; all of the processes essential to the sustainment of the discharge occur in the cathode fall region or very close to the plasma-cathode fall boundary.

In the present discharges the potential of the walls between the anode and the start of the cathode fall is from 10 to 100 times higher than that of the walls surrounding the positive column of the normal glow discharge. Furthermore, the observed energy distribution of electrons incident on the anode shows that electrons from the cathode fall region do not achieve a low drift velocity during their passage through the low-field region near the anode as in ordinary glow discharges. These facts lead to some question as to whether a plasma existed at all in the present discharges.

In an attempt to direct a plasma, a 3-mm hole was

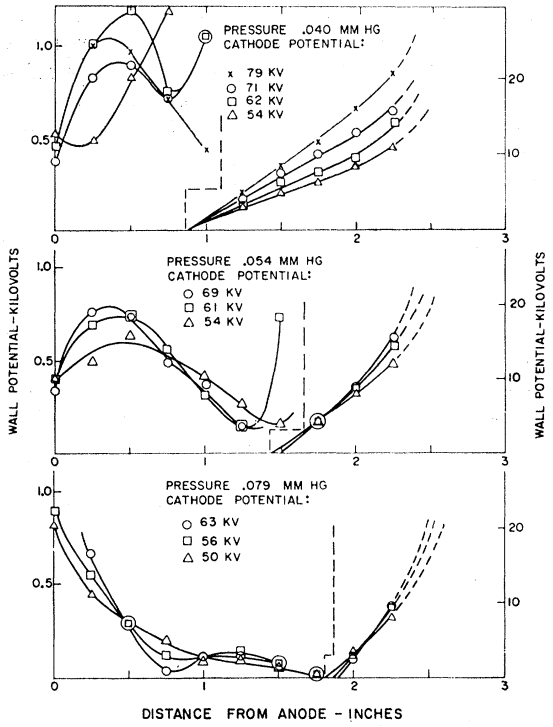

FIG. 13. Wall potential distributions measured under various operating conditions. Potential values are negative and measured relative to anode. Portions of the curves to the left of the dashed lines refer to left-hand ordinate scale and portions of the curves to the right of the dashed lines refer to right hand ordinate scale.

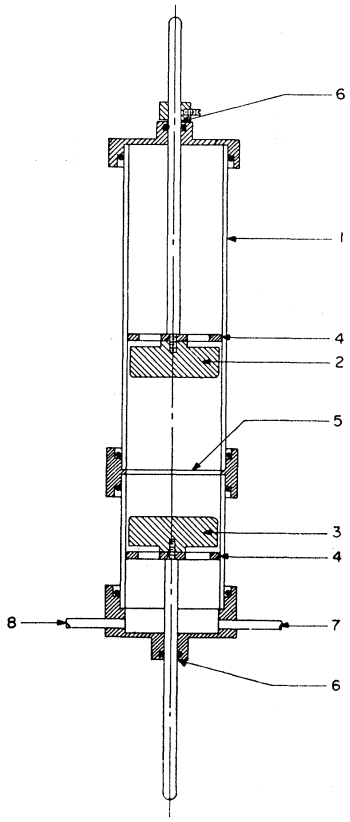

FIG. 12. Tube arrangement used for determination of wall potential distributions. Parts: 1—Pyrex wall, 2—stainless steel cathode, 3—stainless steel anode 4—electrode centering rings, 5—stainless steel ring probe, 6—sliding seals, 7—gas inlet tubulation, 8—vacuum pump tubulation. A thermocouple vacuum gauge connection was made through a third tubulation in the tube base (not shown).

[21] The term "cathode dark space," sometimes used to describe the high-field region of ordinary glow discharges, is inappropriate here because no clearly defined discontinuity in light intensity occurs at the cathode fall boundary in the present discharges.

drilled in the center of the anode and an extraction electrode of the same diameter as the anode was placed 5 cm behind this hole outside the main discharge volume. When the extractor electrode was biased negatively or slightly positively (<40 v) with respect to the anode, a very low current independent of bias voltage was received by the extractor electrode; however, when the bias was increased above 50 v, the total tube current increased from 1 amp to 1.4 amp and over half of the total tube current flowed through the small hole to the extractor. This behavior was interpreted as conclusive evidence of the presence of a dense plasma near the anode since the extraction field at the current transition, ~8 v/cm, could only have penetrated a small distance through the anode aperture and could only have diverted very low-energy electrons from their normal course toward the main anode. The fact that a positive extraction voltage was required to cause the current transition suggests that a negative drop in potential exists between the plasma and the anode in the undisturbed discharge. More convincing evidence of this is presented in the following section.

IX. PROBE INVESTIGATION OF PLASMA

The spatial extent of the plasma and the temperature and density of plasma electrons were determined by means of the Langmuir probe technique. In preliminary experiments the ring electrode used in the wall potential measurements was employed as a probe. An electronic sweep circuit varied the potential of the probe at the rate of 1 v/μsec from any desired base potential in the range -3 to $+0.1$ kv relative to the anode. Probe potential minus this base potential was displayed as the X deflection and the probe current as the Y deflection on an oscillograph screen. A 50-v-wide section of the probe voltage-current characteristic curve could be observed during the steady-state portion of each discharge. Characteristics extending over a wide voltage range could be constructed from separate oscillograph records taken on successive discharges at various base potentials.

The characteristic curves shown in Figs. 14(a) and 14(b) are typical of the data obtained with the ring probe located along the low-potential portion of the glass wall. The potential at which the net probe current is zero is the "floating potential" which the probe would attain if unattached to an external circuit. When the probe potential is negative with respect to floating potential, a net positive current flows to the probe and when the probe potential is positive relative to floating potential, the net current is negative. When the probe approaches within a few volts of anode potential, there occurs an abrupt increase in negative current. This rapid transition is shown in greater detail in the oscillogram of Fig. 14(b). The increase in current between the extreme left end of the figure and the inflection point P is interpreted as due the collection of low-energy electrons from the plasma. A plot of $\log(I-I_0)$ vs V, where I is the net probe current, I_0 is the saturation current, and V is the probe potential, produced a nearly straight line indicating an approximately exponential (Maxwellian) electron energy distribution. The electron temperature determined from the slope is 2.8 ev.

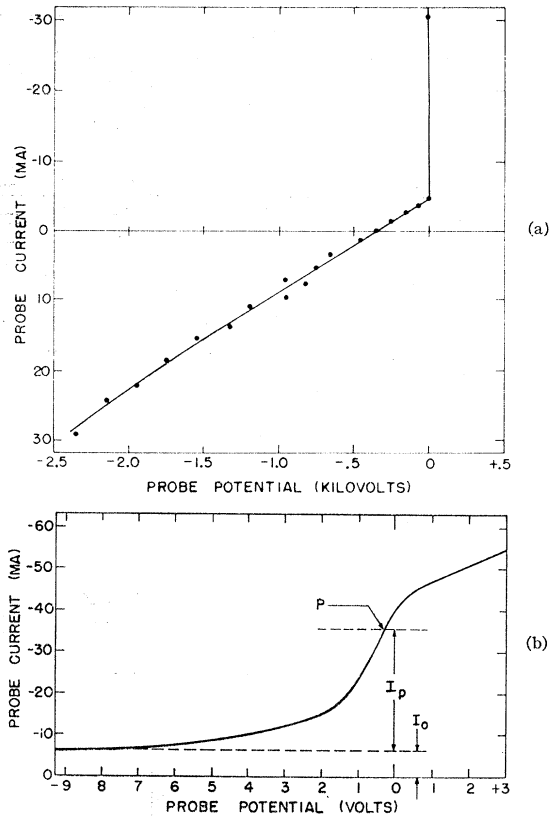

FIG. 14. Probe voltage-current characteristics obtained with the ring probe located $\frac{1}{2}$-in. above the anode. Operating conditions: tube voltage 76 kev, tube current 0.6 amp, pressure 0.037 mm Hg. (a) Probe characteristic at large negative potentials, (b) Expanded plot of probe characteristic near zero potential. Probe potentials are measured relative to the anode.

The total random electron current I_P due to the low-energy plasma electrons is approximately given by the difference between the current at the inflection point P and the saturation current I_0. According to the theory of the plane probe,[22] the electron density in the plasma is given by

$$n=(I_P/A)(2\pi m/kT)^{\frac{1}{2}}, \tag{4}$$

where A is the probe area, m is the electron mass, and kT is the mean energy of the plasma electrons. For the operating conditions corresponding to Fig. 14, the electron density calculated from Eq. (1) is 2.4×10^9 cm^{-3}. This value of n must be regarded as a rather crude

[22] D. Bohm, E. H. S. Burhop, and H. S. W. Massey, *The Characteristics of Electrical Discharges in Magnetic Fields*, edited by A. Guthrie and R. Wakerling (McGraw-Hill Book Company, Inc., New York, 1949), pp. 14 and 82.

estimate since the negative potential of the glass walls directly adjacent to the probe inhibits the collection of plasma electrons from directions other than close to the normal.

To obtain more precise measurements of plasma density, a small plane probe of 0.277 cm² area was mounted on the end of a movable metal tube which protruded into the discharge from a hole in the center of the anode. The support tube was connected to the anode and the probe was connected via a coaxial lead to the voltage and current display circuit used for the wall probe measurements. With this probe, measurements could be made at all points along the central axis of the discharge without disturbance from the negatively charged glass walls. The voltage-current curves were very similar to those taken with the wall probe except for a ten-fold increase in the value of the random electron current density $J_P^- = I_P/A$. Estimates of the plasma temperature and electron density were made as described above and the following results were obtained over a range of operating pressures from 0.039–0.10 mm Hg, applied potentials of 60–80 kv, and tube currents from 0.5 to 7.2 amp:

1. The temperature of the plasma electrons is 2.8 ± 0.6 ev over the entire range of operating conditions surveyed.

2. The random current density J_P^- of plasma electrons is a slowly varying function of position from the anode out to the point where the cathode fall of wall potential begins. Here an abrupt 90% drop in J_P^- occurs in a distance of 5 mm, indicating the end of the plasma and the start of a positive sheath.

3. The mean electron density along the length of the plasma, as obtained from Eq. (4), is directly proportional to the total tube current and follows the empirical relation

$$n = 2.73 \times 10^{10} I_T, \tag{5}$$

where n is in units of cm^{-3} and I_T is the total tube current in amperes.

4. The plasma potential, assumed to be equivalent to the potential at which inflection point occurs in the V-I characteristic, was determined to an accuracy of ± 10 v. Within this range of uncertainty the potential throughout the length of the plasma was equal to the potential of the anode.

5. The random electron current density J_P^-, averaged over the length of the plasma, is proportional to the total tube current and follows the empirical relation

$$J_P^- = 0.123 I_T, \tag{6}$$

where J_P^- is in units of amp/cm² and I_T is in amperes.

In view of the constancy of the electron density along the length of the plasma, it seems reasonable to assume that the density is also constant from side to side. On the basis of this assumption the plasma would emit an approximately uniform current density of ions to the walls and to the cathode fall region. As both the cathode and the walls are at negative potentials relative to the inside of the plasma, a positive sheath must form between the plasma surface and these boundaries. It has been shown[22] that the positive-ion current density J_P^+ flowing from a plasma into such a boundary sheath is given by

$$J_P^+ = 0.40 n (2kT/M)^{\frac{1}{2}}, \tag{7}$$

where n is the plasma electron density, kT the mean energy of the plasma electrons, and M the mass of the positive ions. Assuming the pertinent ions to be D_2^+ and substituting the measured values for n and kT, one finds

$$J_P^+ = 1.02 \times 10^{-3} I_T, \tag{8}$$

where J_P^+ is in units of amp/cm². The wall sheath thickness d is given by the Child-Langmuir equation,

$$d = \left[\frac{1}{9\pi} \left(\frac{2e}{M} \right)^{\frac{1}{2}} \frac{V^{\frac{3}{2}}}{J_P^+} \right]^{\frac{1}{2}}, \tag{9}$$

where e is the electron charge, and V is the potential drop across the sheath. Substituting Eq. (8) and evaluating the constants gives

$$d = 5.2 \times 10^{-3} V^{\frac{3}{4}} / I_T^{\frac{1}{2}}, \tag{10}$$

where V is in volts, I_T is in amp, and d is in cm. For a tube current of 1 amp and a wall potential of 200 v, $d = 0.28$ cm. The wall sheath may be considered to be thin compared to the tube diameter for most of the operating conditions encountered in these experiments.

A very important parameter of the discharge is the ion current from the plasma into the cathode fall. If one considers the cathode end of the plasma as occupying the full diameter of the tube, this current is given approximately by the product of J_P^+ by the cross-sectional area of the tube. Using Eq. (8) one then obtains for the current into the cathode fall

$$I_P^+ = 0.0204 I_T. \tag{11}$$

Denoting the secondary electron current from the cathode as I_K^- and the mean secondary emission per ion as $\bar{\gamma}'$, we have

$$I_T = (1 + 1/\bar{\gamma}') I_K^-. \tag{12}$$

Setting $\bar{\gamma}' = 14.1$ (see Sec. VI) and combining Eqs. (11) and (12) gives

$$I_P^+ = 0.022 I_K^-. \tag{13}$$

The importance to the cathode fall mechanism of an ion supply from the plasma of this magnitude may be seen by comparing I_P^+ with the rate of ion generation in the cathode fall due to secondary electrons from the cathode. In Fig. 15 is plotted the electron ionization cross section vs electron energy based on the low-energy data of Tate and Smith[23] (energy <750 ev) and the

[23] J. T. Tate and P. T. Smith, Phys. Rev. 39, 270 (1932).

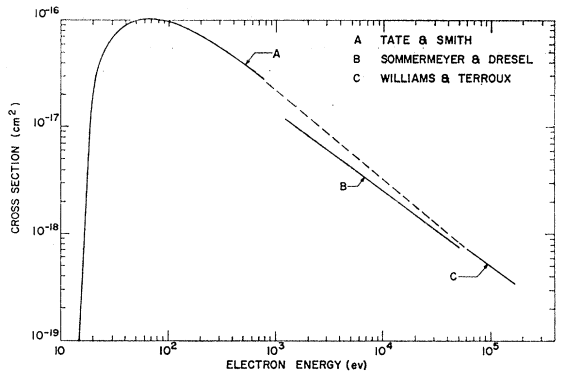

FIG. 15. Cross section for electron ionization of hydrogen gas vs electron energy.

high-energy data of Williams and Terroux[24] (energy >60 kev). The author's interpolation between these two sets of data lies somewhat above the experimental curve of Sommermeyer and Dresel.[25] If one assumes a linear variation of the space potential between the cathode and the start of the cathode fall, a total potential drop of 80 kv, and negligible energy loss of electrons in the cathode fall region due to inelastic collisions, the rate I_A^+ of ion production in the cathode fall due to cathode secondaries is found to be

$$I_A^+=0.024I_K^-. \tag{14}$$

It is therefore apparent that the ion current I_P^+ from the plasma into the cathode fall is of the same order of magnitude as the direct production I_A^+ by electrons in the cathode fall. Although the assumption of a linear spatial variation of potential in the cathode fall gives rise to some error in the calculated value of I_A^+, any deviation from linearity is probably in such a direction as to make the actual value of I_A^+ lower than the estimated value.

The floating potential of the glass walls surrounding the plasma is extraordinarily high in these discharges. This is believed to be due to the entrance into the plasma region of high-energy electrons from the cathode fall. As indicated by the results of Sec. VII, a stream of electrons, consisting mainly of a monoenergetic group which originates at the cathode, pass through both the cathode fall and the plasma virtually without energy loss due to collision and also without appreciable gas scattering. The major part of the tube current is carried by these fast electrons (~93%). Some of this energetic stream may strike the walls directly, but a large fraction is backscattered from the anode at large angles so as to strike the walls in the plasma region. From the available experimental data on electron backscattering[26] it has been estimated that the current density of backscattered electrons to the walls surrounding the plasma in the present discharges is of the order of

$$J_B^-=2.8\times10^{-3}I_T, \tag{15}$$

where J_B^- is in amp/cm² and I_T is in amperes. This current density is ~2.8 times larger than the estimated positive ion current density to the walls given by Eq. (8). Hence it is clear that the backscattered electrons have a controlling influence on the steady-state potential of the walls around the plasma.

In order for wall potential equilibrium to occur, as in the quasi-steady portion of the discharge, it is necessary that a negative current density of magnitude $(J_B^- - J_P^+)$ flow away from the walls. [If the charge from the current $(J_B^- - J_P^+)$ were permitted to accumulate without compensation, the potential of the walls would change at the rate of $\sim 2\times10^3$ v/μsec contrary to observation.] The most likely source of the required balancing current is secondary emission from the walls due to the impact of the fast electrons and ions comprising the currents J_B^- and J_P^+. If one assumes that the secondary emission coefficients for glass are of the same order of magnitude as those for metals, it can be shown that the secondary electron current is of the proper order of magnitude to give charge balance. However, additional data on secondary emission from glass must be obtained before this point can be settled.

One of the more important questions concerning mechanism of the discharge is that of the mode of ion production in the plasma region. In order to examine this point in detail it is useful to consider a particular operating condition. Consider, for example, the operating condition $V_T=80$ kv and $p=0.060$ mm Hg. Here the cathode fall length is 3.6 cm [Eq. (3)] and the plasma, which fills the remainder of the tube, is 4.0 cm long. The net positive ion flow out of the plasma, to the walls, to the cathode fall, and to the anode,[27] is equal to the net surface area concerned times the ion current density J_P^+. This current,

$$I_W^+=0.102I_T, \tag{16}$$

is the ion production rate within the plasma neglecting losses due to recombination.

The ion production within the plasma due to electrons from the cathode fall region has been calculated by averaging the electron ionization probability (calculated from Fig. 15) with respect to the electron spectrum shown in Fig. 10. For the assumed operating conditions this production rate is

$$I_C^+=0.0078I_T. \tag{17}$$

[24] E. J. Williams and F. R. Terroux, Proc. Roy. Soc. (London) A126, 289 (1929).

[25] K. Sommermeyer and H. Dresel, Z. Physik 141, 307 (1955).

[26] The gross backscattering coefficient and energy distribution of backscattered electrons (from Fe) were taken from E. J. Sternglass, Phys. Rev. 94, 345 (1954). The angular distribution of backscattered electrons was assumed to follow the cosine law; see H. Kulenkampf and K. Ruttiger, Z. Physik 137, 426 (1954).

[27] We include here the positive ion flow to the anode which would be present in case of a negative anode fall. The "sign" of the anode fall is discussed at the ends of Secs. VIII and IX.

A comparison of Eqs. (16) and (17) shows that I_W^+ is more than an order of magnitude greater than I_C^+. Hence, an additional ionizing mechanism is apparently required to explain the plasma ion production. It is very likely that most of the required additional production comes from secondary electrons emitted from the glass walls. Although these electrons are ejected with very low initial energies, they are accelerated in the positive ion sheath at the walls so as to enter the plasma with energies of the order of 0.1 to 1.0 kev, depending on the local wall potential. If one assumes that the secondary electron current density emitted at the walls is given by $J_B^- - J_P^+$, the net current of secondaries from the wall is found to be

$$I_S^- = 0.113 I_T. \tag{18}$$

The ion production rate remaining to be accounted for is

$$I_W^+ - I_C^+ = 0.094 I_T. \tag{19}$$

To account for the remaining ions in terms of ionization due to wall secondaries it is necessary that the wall secondaries produce, on the average, $0.094/0.113 = 0.83$ ion pairs within the plasma. For a mean electron energy of 0.5 kev (corresponding to the mean wall potential for the assumed operating conditions) the electrons are required to traverse a path length of about twice the tube diameter to produce the required number of ions. Considering the possibility of reflections of the wall secondaries from the retarding potential barrier surrounding the plasma, such a path length seems entirely within reason. Very tedious calculations taking into account the scattering of the wall secondaries in the gas and the relative probabilities of collection and reflection at the glass walls would be required to give exact quantitative proof of sufficiency of the proposed ionization mechanism. Such calculations have not thus far been attempted; however, the above arguments show that wall secondaries are definitely a first-order source of plasma ionization.

A steady-state charge balance in the plasma can only occur if the loss of positive ions, given by I_W^+ [Eq. (15)], is balanced by the random electron current to the anode. If J_P^-, the measured random current density of plasma electrons, were permitted unrestricted flow to the anode, the loss of electrons from the plasma would be 24 times the loss of ions. It is concluded that the anode must be sufficiently negative with respect to the plasma to restrict the electron flow to 1/24 the random current density. This implies (for an electron temperature of 2.8 ev) a *negative* anode fall of the order of 9 v. In an ordinary glow discharge at higher pressure, a positive anode fall suffices to provide charge balance because the influx of low-energy electrons from the cathode fall region balances the loss to the anode. In this instance the positive ion loss from the plasma to the walls and to the cathode fall is supplied by ionization produced by electrons during their passage across the positive anode fall zone.

X. COLLISION PROCESSES IN THE CATHODE FALL REGION

On the basis of the foregoing discussion it is clear that ion production occurs throughout the length of the cathode fall due to ionizing collisions of cathode secondary electrons. The net ionization probability per electron is so small (~ 0.02) that the cathode electrons move through the cathode fall region virtually as in free fall through a vacuum. Most of the electron ionization occurs very close to the cathode surface where the electron energy is low and the ionization cross section is high. Owing to the continual acceleration of the cathode electrons, the assumption of a constant electron ionization cross section throughout the cathode fall region (Neu[4]) is completely inapplicable here.

It has been shown (Sec. IX) that the ion influx to the cathode fall region from the plasma boundary is comparable to the electronic ion production in the cathode fall. The ions from the plasma travel, on the average, a much greater distance in the high-field region than the ions produced directly by electrons from the cathode. Consequently, the plasma ions, together with the secondaries they produce while en route to the cathode, produce the majority of the cathode secondaries.

The secondary effects produced by ions during their traversal of the cathode fall region include charge exchange, ionization, and dissociation. Of the three processes, charge exchange is the most probable. The cross section for charge exchange[9,19] is approximately constant for D_2^+ ions in the energy range 1–50 kv, and the mean free path is approximately one-fifth the length of the cathode fall. If one assumes a uniform field throughout the cathode fall, a D_2^+ ion will attain a mean energy of $\frac{1}{5}$ the cathode-fall potential drop before undergoing a charge exchange collision. When such a collision occurs the primary ion is converted to a fast D_2 neutral (or two fast D atoms) and a new D_2^+ ion starts from rest, repeating the same process. Thus a D_2^+ ion from the plasma gives rise to a "charge-exchange cascade" which contains upon arrival at the cathode a single D_2^+ ion and five to ten neutrals. The D_2^+ ions and D_2 neutrals will have a mean energy of $\frac{1}{5}$ the cathode fall potential drop and the D neutrals will have an energy of about $\frac{1}{2}$ this great. This argument provides a crude explanation of the observed mean energy of the D_2^+ ions incident on the cathode (Sec. IV).

The development of the charge-exchange cascade is complicated by ionizing collisions of the constituent particles with gas molecules. According to the available data on ionization due to neutrals and ions of 10–20 kev kinetic energy,[20,28,29] the ionization mean free path is of

[28] J. P. Keene, Phil. Mag. **40**, 369 (1949).
[29] V. V. Afrosimov, R. N. Ilin, and N. V. Fedorenko, Soviet Phys.—JETP **34**, 968 (1958).

the order of the cathode fall length, thus the size of the cascade is substantially augmented by the production of additional ions along its path. Some modification of the cascade is also introduced by dissociation in flight of D_2^+ ions to form D^+ ions,[9,30] and electron loss from fast D neutrals.[20,31] Both of these processes have mean free paths of the order of the cathode fall length.

Detailed consideration of the net effect of all of these processes on the energy distribution of the particles incident on the cathode, together with a self-consistent treatment of space charge, will be presented in Part II.

XI. CONCLUSIONS

The high-voltage glow discharge has been experimentally examined and is found to be partitioned, along the direction of the electric field, into an anode fall region, a plasma region, and a cathode fall region. All but about 10 v of the applied potential appears across the cathode fall zone. The potential drop across the anode fall region is approximately 9 v (negative relative to the plasma) and the plasma potential varies not more than 10 v from end to end. The glass walls surrounding the lateral boundaries of the plasma attain a potential of the order of 0.1 to 1.0 kv relative to the interior of the plasma due to bombardment by fast electrons backscattered from the anode. Ion production in the plasma is caused, in large part, by secondary electrons released from the glass walls due to fast electron and positive ion bombardment. Electrons are emitted from the cathode by both positive ion and neutral atom bombardment. These electrons pass through the entire length of the discharge with very little energy loss or scattering due to collisions. The ion production in the cathode fall region by cathode electrons is comparable to the ion flow from the plasma into the cathode fall. Ions moving from the plasma into the cathode fall give rise to complex "charge-exchange cascades" involving the production of 5 to 10 secondary neutral atoms and molecules having mean energies corresponding to about $\frac{1}{5}$ the cathode fall potential drop. The fast heavy particles within these cascades initiate secondary cascades by ionizing gas molecules.

Both the plasma and the cathode fall regions of the present discharges require vastly more complex methods for their complete mathematical description than the methods heretofore used in the case of lower-voltage "normal" and "abnormal" glow discharges. The present results provide a fairly detailed conceptual framework for the construction of the required, more advanced theory.

[30] N. V. Fedorenko, V. V. Afrosimov, R. N. Ilin, and D. M. Kaminker, Soviet Phys.—JETP **2**, 267 (1959).
[31] P. M. Stier and C. F. Barnett, Phys. Rev. **103**, 896 (1956).

ACKNOWLEDGMENTS

It is a pleasure to thank B. A. Wickesburg, D. L. Allensworth, D. G. Schreiner, and R. T. McVeety for assistance in the design and construction of the experimental apparatus. The author is indebted to L. B. Loeb for several helpful discussions concerning the interpretation of the measurements.